New Journal of Physics
The open access journal at the forefront of physics

Deutsche Physikalische Gesellschaft DPG
IOP Institute of Physics
Published in partnership with: Deutsche Physikalische Gesellschaft and the Institute of Physics

CrossMark

OPEN ACCESS

RECEIVED
14 October 2022

REVISED
27 February 2023

ACCEPTED FOR PUBLICATION
8 March 2023

PUBLISHED
20 March 2023

PAPER

Exciton-polariton dynamics of the single site-controlled quantum dot-nanocavity in the coexisting strong-weak coupling regime

Jiahui Huang[1,3,*], **Wei Liu**[1,3,*], **Murat Can Sarihan**[1], **Xiang Cheng**[1], **Alessio Miranda**[2], **Benjamin Dwir**[2], **Alok Rudra**[2], **Eli Kapon**[2] **and Chee Wei Wong**[1,*]

[1] Department of Electrical and Computer Engineering, Mesoscopic Optics and Quantum Electronics Laboratory, University of California, Los Angeles, CA 90095, United States of America
[2] Laboratory of Physics of Nanostructures, École Polytechnique Fédérale de Lausanne (EPFL), Lausanne, Switzerland
[3] These authors contributed equally.
[*] Authors to whom any correspondence should be addressed.

E-mail: jiahuihuang@ucla.edu, weiliu01@lbl.gov and cheewei.wong@ucla.edu

Keywords: site-controlled quantum dot, exciton polaritons, cavity electrodynamics, nanophotonics

Supplementary material for this article is available online

Abstract
Deterministic positioning single site-controlled high symmetric InGaAs quantum dots (QDs) in (111)B-oriented GaAs photonic crystal cavities with nanometer-scale accuracy provides an idea component for building integrated quantum photonic circuits. However, it has been a long-standing challenge of improving cavity *Q*-factors in such systems. Here, by optimizing the trade-off between the cavity loss and QD spectral quality, we demonstrate our site-controlled QD-nanocavity system operating in the intermediate coupling regime mediated by phonon scattering, with the dynamic coexistence of strong and weak coupling. The cavity-exciton detuning-dependent micro-photoluminescence spectrum reveals concurrence of a trend of exciton-polariton mode avoided crossing, as a signature of Rabi doublet of the strongly coupled system. Meanwhile, a trend of keeping constant or slight blue shift of coupled exciton–cavity mode(CM) energy across zero-detuning is ascribed to the formation of collective states mediated by phonon-assisted coupling, and their rare partial out-of-synchronization linewidth-narrowing is linked to their coexisting strong-weak coupling regime. We further reveal the pump power-dependent anti-bunching photon statistical dynamics of this coexisting strong-weak coupled system and the optical features of strongly confined exciton-polaritons, and dark-exciton-like states. These observations demonstrate the potential capabilities of site-controlled QD-cavity systems as deterministic quantum nodes for on-chip quantum information processing and provide guidelines for future device optimization for achieving the strong coupling regime.

1. Introduction

Solid-state quantum-confined light-matter interactions serve as a critical resource for unbreakable secure quantum communications [1–5] and long-distance quantum communications through a trusted repeater node architecture [6–9]. Progress in this area based on InGaAs quantum dots (QDs) has been guided by demonstrations of on-demand bright single photon sources [10–12], achieving strong coupling regime in high-quality factor (*Q*) microcavities [13–25], deterministic coupling single QDs in single CMs [26], entanglement generation [7, 27–30], and coherent control [15, 18, 31, 32]. Moreover, recent studies on the quantum network protocol based on deterministic cluster state generation [30, 33–35] and solid-state quantum memory enabled single-photon switching [9, 18] received considerable interest. In particular, cavity-enhanced biexciton-dark-exciton cascaded system in GaAs-based QDs [36, 37] is emerging as a promising platform to realize such a protocol. Crucially, pure dephasing of two-level systems, defined as any disruption of quantum state without causing population relaxation but introducing random phase evolution, plays a fundamental role in error-tolerant networks [38] and frequency-stabilized on-chip scalable indistinguishable single photon emitter [39, 40] for on-chip quantum information processing (QIP). In GaAs-based QDs, the main pure dephasing mechanisms, resulting in spectral broadening, are related to rapidly fluctuating electrical charges [41] and carrier-phonon interactions [42–47]. In the weak coupling regime, pure dephasing mediated Purcell effect assists a large fraction of the QD emission to be channeled into the CM, leading to efficient off-resonance cavity feeding up to a few meV detuning [41, 48, 49]. At the same time, finite coupling between QD exciton and cavity can also manifest the emission of cavity photons at the QD exciton energy such as in a dissipative cavity where the cavity loses photons at a rate much faster than the QD [48, 50]. Alternatively, in the strong coupling regime, the vacuum Rabi splitting and polariton state is modified by the damped coherent Rabi oscillations induced by pure dephasing [51]. Apart from the clear distinction between strong and weak coupling, recent studies indicate the possibility of the *intermediate* coupling regime, which shares the coexisting features of both strong and weak coupling, as observed in self-assembled GaAs-based QDs in micropillar [52] and PhC cavities [53]. Specifically, recent theoretical studies suggest that phonon-assisted QD-cavity interaction plays an important role in this intermediate coupling regime [43, 44]. This suggests the importance of investigating pure dephasing in such cavity quantum electrodynamical systems for achieving practical QIP with suppressed environmental fluctuations.

Particularly the intrinsic pure dephasing of the two-level system in QDs and its interaction with the cavity remains to be difficult to access. This is because most studies rely on the self-assembled Stranski–Krastanov (SK) QDs, which induce spurious cavity feedings related to their wetting layer [54]. Consequently, the hybridization of localized self-assembled QD states with delocalized wetting layer states results in broadband quasi-continuum states that give rise to a background emission [55, 56]. More importantly, the random SK QDs nucleation leads to difficulty in precisely positioning QDs at the desired location in the cavity which crucially affects the physical properties of incorporated QDs and thus the interaction with cavities. Alternatively, precise positioning of single site-controlled highly symmetric pyramidal InGaAs QDs in PhC cavities with nanometer scale accuracy holds unique advantages compared to self-assembled QDs due to its deterministic nucleation therefore the creation of large-scale arrays of similar QD-cavity is achievable [57, 58]. Its growth mechanism also avoids spurious cavity feeding thanks to the absence of wetting layers [57, 58], which is beneficial for studying the intrinsic interaction between emitter and cavities. Furthermore, single photon generation and processing in integrated quantum photonic circuits require the incorporation of several QDs in cavities, waveguides, or more complicated photonic structures which cannot be accomplished reliably with self-assembled QDs.

However, to our knowledge, previous experimental studies of site-controlled InGaAs QD-cavity systems are limited to the weak coupling regime, such as [48, 59]. This can be due to the fact that PhC cavities based on (111)B-oriented GaAs substrate, which is for etching high symmetric inverted pyramids for site-controlled InGaAs QD epitaxy, usually exhibit larger losses than conventional (100)-oriented geometry. These studies report a relatively low cavity Q-factor of $\sim$2500 at QDs s-shell emission wavelength of $\sim$860 nm [48, 59]. In the present study, with the optimization of the Indium content and pyramid size of our single site-controlled InGaAs QD—$L3$ PhC cavities, we tailored the QDs s-shell emission wavelength to a longer wavelength towards $\sim$1 μm where a reduced cavity loss can be obtained, while maintaining the sub-100 μeV narrow excitonic linewidth. We observed an improved Q-factor of (111)B-oriented PhC cavity larger than $\sim$4200, thanks to the lesser influence of absorption losses from the Urbach tails of GaAs [60, 61], and smaller structural disorders due to larger structural parameters [62]. Based on our tailored device, we achieve the intermediate coupling regime and systematically investigate the related phonon-mediated coupling and carrier recombination dynamics, using high-resolution polarization-resolved micro-photoluminescence (μPL), time-resolved PL (TRPL), and second-order photon correlation measurements. We reveal the pump power-dependent anti-bunching photon statistical dynamics of the coexisting strong-weak coupled system and the optical features of strongly confined exciton-polaritons and dark-exciton-like states.

The singe site-controlled pyramidal QDs, grown on the (111)B-oriented GaAs substrate, are located at the apex of highly symmetric inverted pyramidal pits and incorporated within PhC cavities written on top (refer to supplementary section I for detail). Our single site-controlled QD-cavity system is studied via micro-photoluminescence (μPL). The sample is mounted on the cold finger of a liquid helium flow cryostat, positioned accurately with piezoelectric actuators in the xy-direction. An integrated image system with a tungsten-halogen lamp is used for visualizing the QD-cavity and the laser spot. The sample is excited by either a continuous wave (CW) low-noise diode-pumped solid-state laser at 532 nm, or a 900 nm pulsed diode laser with $\approx$100 ps pulse duration. A 100$\times$ microscope objective with a numerical aperture of 0.7 allows a $\approx$1 μm diffraction-limited pump beam spot size on the sample. The μPL signals are collected and collimated by the same objective and refocused onto the entrance slit of a 1 m spectrometer with 1200 grooves cm^{-1}, enabling a high spectral resolution of 8 pm (10 μeV). A liquid nitrogen-cooled

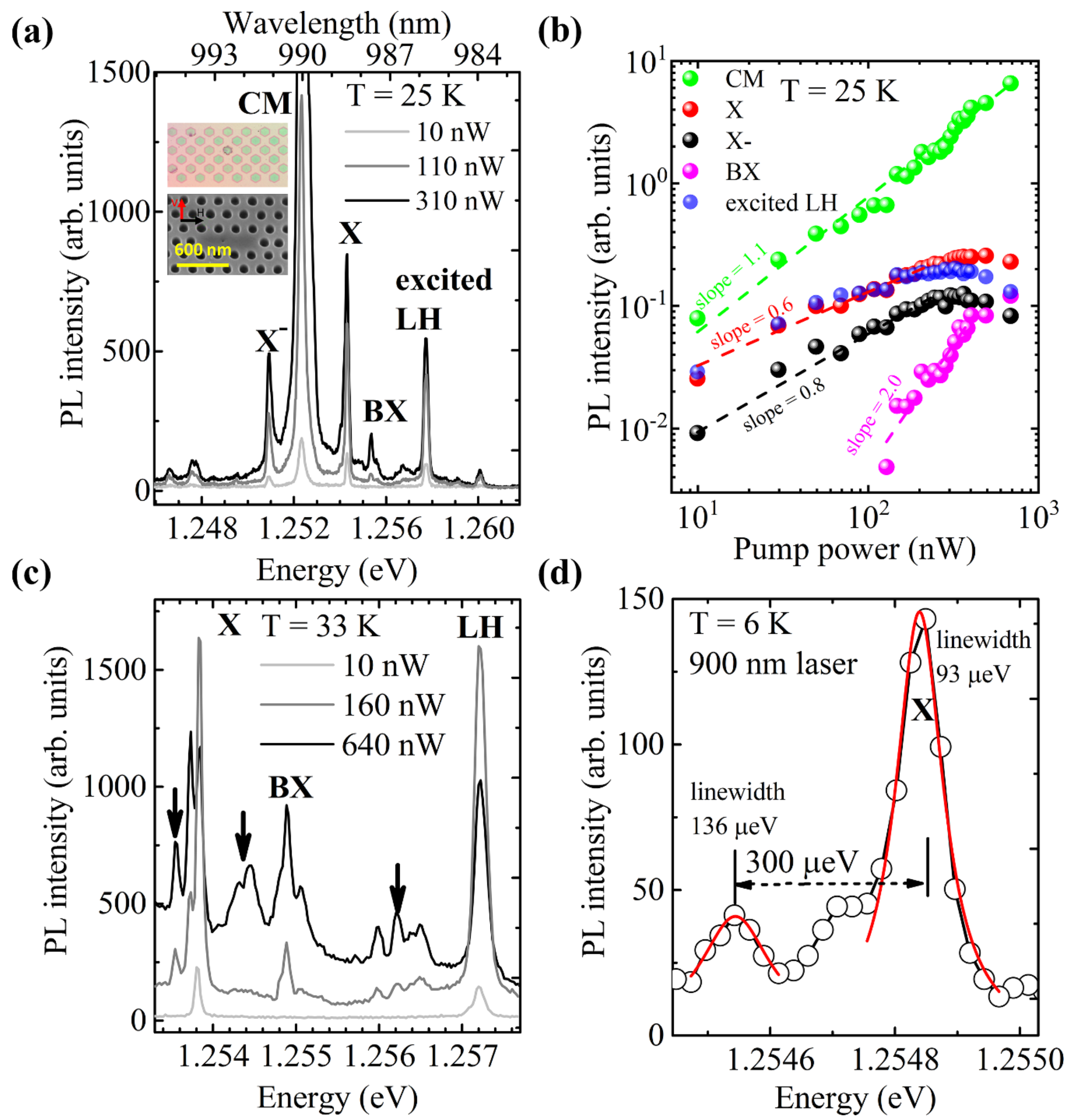

Figure 1. Exciton complexes and dark excitons in single site-controlled InGaAs cavity quantum electrodynamics. (a) μPL spectrum of a single pyramidal InGaAs QD-*L*3 PhC cavity system at 25 K with 532 nm non-resonant pumping at 10 nW, 110 nW, and 310 nW. Inset: an image of the PhC cavity. Scale bar: 600 nm. (b) Integrated μPL intensity of different QD exciton species and cavity mode as a function of pump power at 25 K. (c) A zoom-in of the exciton complex species marked by arrows at 33 K (near the X and BX emission) with 532 nm non-resonant pumping at 10 nW, 160 nW, and 640 nW. (d) Sample zoom-in of the peak 300 μeV below X emission, at 6 K with 900 nm pumping.

charge-coupled device attached to the axial exit of the spectrometer acquires the PL spectrum. A fiber-coupled Hanbury–Brown and Twiss (HBT) setup sitting on a precision optical rail comprising of a 50:50 single mode fiber beamsplitter and feed two fiber-coupled Si avalanche single-photon detectors with 25 Hz dark counts. Tunable long and short pass filters are combined as a narrow band pass filter before the fiber coupler. Time-correlated single-photon counting is implemented for acquiring the second-order correlation (g^2) and TRPL measurements. Polarization-resolved μPL is performed by implementing a half-wave plate and a linear polarizer in front of the spectrometer entrance. The linear polarizer is fixed at the polarization orientation which corresponds to the maximum reflectivity of the grating spectrometer as well as the cavity main polarization direction. The measurement setup schematic and the FDTD modeling of the PhC cavity are detailed in supplementary section I.

1.1. Pure dephasing and exciton complexes in the single site-controlled InGaAs QD-PhC cavity

Figure 1(a) presents the resulting excitonic emissions from a single pyramidal InGaAs QD and the *L*3-PhC CM at 25 K with X-CM detuning ≈2 meV, excited non-resonantly by the 532 nm laser. As labeled in figure 1(a), the *s*-state excitonic emission [57, 58] consists of a complex of the negatively-charged exciton (X^-), neutral exciton (X), biexciton (BX), and likely an excited light hole (LH) state. It is worth noting that the QD s-state emission is around 1.252 eV (990 nm) which suggests lesser influences from the Urbach tails of GaAs bandgap [60, 61] in this device. The relative binding energies [63] of the BX and X^- with respect to X are -1.06 meV and 3.41 meV respectively. The pronounced X^- population even at low excitation of 10 nW is mainly due to background-doping donors, incorporated during growth. Moreover, as a contributing factor, the significant asymmetric mobility between electron and hole further favors the formation of X^-, rather than the positively charged exciton (X^+) [64]. At the low excitation regime, (<150 nW), the full-width half-maximum (FWHM) linewidths of the X^-, X, BX, and LH transitions are nearly constant with $\gamma_{X-} = 173 \pm 9\ \mu$eV, $\gamma_X = 143 \pm 10\ \mu$eV, $\gamma_{XX} = 117 \pm 42\ \mu$eV, and $\gamma_{LH} = 202 \pm 5\ \mu$eV respectively, extracted by Lorentzian fitting. It is apparent that the linewidth broadening is larger than the Fourier transform limits of the typical QD nanosecond lifetime ($\approx$7 μeV), suggesting the contribution of pure dephasing via fluctuating environmental charges. Though phonon scattering can contribute to the broadening, it is not expected to be dominant below 50 K [65]. The larger linewidth observed at low excitation for X^- compared to X can be understood by its additional charge carriers which have increased Coulomb interactions with fluctuating environmental electric fields. We note that γ_{X-} monotonically decreases by $\approx$30 μeV as excitation increases from 200 to 700 nW, which is due to the saturation of the local charge states. Meanwhile, the significantly larger γ_{LH} is caused by a more delocalized LH state, experiencing stronger surrounding charge fluctuations. Apart from the excitonic emission, the CM line has a FWHM of κ_{CM} of 296 $\pm$ 12 μeV (Q factor $\approx$4230), which is in the dissipative cavity regime of $\kappa_{CM} \gg \gamma_{exciton}$, where κ_{CM} and $\gamma_{exciton}$ are the cavity loss and QD radiative decay rates respectively.

It is worth pointing out that the absence of a 2D wetting layer in our single pyramidal QD growth rules out far-off-resonance cavity feeding by a spurious emission background. Furthermore, though the pyramidal QD nucleates in the vicinity of three 1-dimensional ridge quantum wires at the wedges of the pyramid, the quantum wire influence is shown to be negligible for low QD excitation powers, owing to the large energy difference and absence of hybridization between the localized QD states and 1D delocalized state and the lower mobility of charges in the disordered 1D barrier. To further verify the above assignment of each sharp transition line, figure 1(b) presents the pump power-dependent μPL at 25 K. The pump power-dependent integrated μPL intensity of X, X^- and LH in logarithmic scale [58] reveals a sublinear slope of 0.6 $\pm$ 0.1, 0.8 $\pm$ 0.1, and 0.6 $\pm$ 0.1 respectively, correlated with the CM increase. In contrast, the far-off resonance BX has the distinctive 2.0 $\pm$ 0.2 slope and features a saturation pump power larger than other excitonic emissions. In addition, the off-resonance CM as a function of pump power shows a slope of 1.1 $\pm$ 0.1.

By further increasing the pump power, additional lines appear next to the BX and X transitions (labeled with arrows in the magnified figure 1(c)), which are likely due to charged exciton complexes and possible recombination of ground state QD electrons with higher-order QD hole states, which have small (<meV) energy spacings. Particularly the sharp emission line slightly below the BX line exhibits a super-linear power-dependent behavior, which suggests the decay of a negatively-charged biexciton (BX^-) [66] or excited biexcitonic states [67]. In addition, the dense lines $\approx$1 meV blue-shifted from the BX represent apparently positively-charged complexes [68]. This can be attributed to the fact that the QD hole capture rate is proportional to the excitation power [69]: the enhanced direct hole capture by the QD at stronger excitation changes the population from negatively charged to neutral X and, with further hole capture, eventually to an X^+. Moreover, it is interesting to observe an additional sharp shoulder redshifted from X at sub-barrier pumping measured at 900 nm, noted in figure 1(c). This is further detailed in the high-resolution spectrum of figure 1(d), measured at 6 K. Particularly it reveals an excitonic species at a transition energy $\approx$300 μeV below the X line (figure 1(d)), which matches the reported exchange interaction induced splitting between the bright and dark excitons (DX) [36]. However, the appearance of charged complexes (1.2547 eV) can overlap and alter their power-dependent behavior. We thus investigate the power-dependent characterization of the DX-like state in another QD-cavity device with the absence of charge complexes detailed in supplementary section II. We note that the residual optical activity of the DX is attributed to the mixing of the heavy hole ground state with the LH component through slightly-reduced QD symmetry [36, 70, 71], which results in a small in-plane polarized dipole moment and partially relieving the spin conservation.

To gain further insights into the interaction between the cavity and QD, as shown in figure 2(a), we carefully tune the X-CM coupling of the same QD-cavity studied in figure 1 with fine-sweeping down to $\approx$300 mK temperature steps in our cryostat, while driving the sub-barrier excitation at 900 nm which suppresses charge fluctuation induced linewidth broadening of X due to the above GaAs bandgap excitation. Figure 2(b) presents the X and CM peak energy as a function of temperature extracted from the spectral Lorentzian fits, with the X-CM coupling occurring around 47 K. Single Lorentzian fittings are used for $T = 46.55$ K and 47.1 K because of the indistinguishable overlap between the X and CM spectra. We witness that the slope of the temperature-dependent CM energy experiences dramatic changes from 44.8 K to 46.3 K which corresponds to a detuning range of 75 μeV $< \delta <$ 120 μeV, where $\delta = \omega_0 - \omega_c$ with ω_0 and ω_c as the X

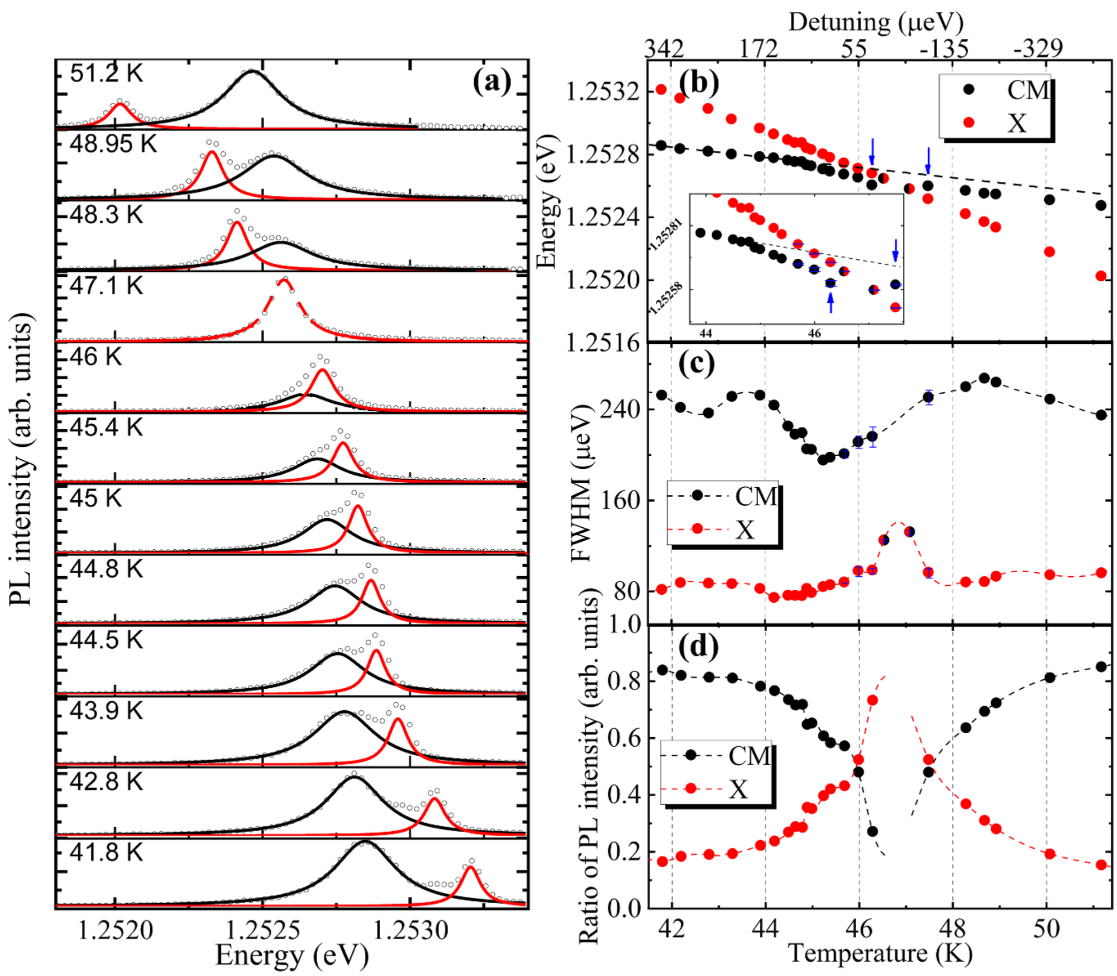

Figure 2. Observations of the coexisting strong-weak coupling regimes probed by high-resolution cryogenic spectroscopy and stepped temperature dependent μPL. (a) Temperature-dependent μPL traces of CM and X emission. (b) Peak energy of CM and X emission as a function of temperature extracted by spectral Lorentzian fitting of a. The black dashed line indicates the slopes of CM at large X-CM detuning. Inset: zoom-in of the mode crossing. (c) Linewidth of CM and X as a function of temperature. The partial out-of-the synchronization linewidth averaging supports an intermediate coupling region mediated by phonon scattering, with a collective state emission. (d) Ratio of the integrated CM and X emission intensity as a function of temperature. Half black and red circles near zero detuning are from single Lorentzian fits. Black and red dash lines are guides to the eyes. Measurements are with 900 nm pulsed excitation.

transition and CM energies. The manner in which its slope changes suggest a trend of an avoided crossing of CM from X. Meanwhile, near zero-detuning, the CM energy remains unchanged within the spectral fitting error when temperature increased from 46.3 K to 47.5 K (data marked by the blue arrow in figure 2(b)). The temperature-dependent CM energy recovers its slope at far detuning. As shown in figure 2(c), the CM and X linewidths show a tendency of becoming equal when approaching the zero-detuning temperature, albeit the CM linewidth minimum does not appear at the same detuning as the X linewidth maxima. It is worth pointing out that the detuning range where the CM linewidth is minimized corresponds to its dramatic slope changing at positive detuning. Meanwhile, the X linewidth maximum occurs at the position where the CM energy is crossing the X line figure 2(d) further presents the ratio of integrated PL intensity of CM (and X) to the total intensity, indicating their inversion with each other as QD-CM coupling is controlled from far-detuning to resonance. The double and single Lorentzian fitting of the μPL at temperatures around the blue arrows in figure 2(b) is detailed in supplementary section III.

We note that the observed slope distortion of temperature-dependent CM energy appears in a small detuning range (<120 μeV) from 44 K to 46 K. Importantly, the observed behavior of avoided-like crossing of CM *deviates from the mode pulling effect* (namely, a tendency of CM energy shifting towards X near resonance), the latter of which results from the spectral overlaps of a low-Q CM and the X phonon sideband [72], in the weak coupling regime. Moreover, the avoided crossing trend of the CM cannot be reproduced by the simple spectral overlaps between CM and X with bulk phonon dispersion as in the weak coupling regime. Instead, the co-occurrence of QD-CM avoided crossing, the unchanged CM energy crossing X, and their partial out-of-synchronization linewidth averaging points to the effect of intermediate coupling mediated by phonon scattering. In this intermediate coupling regime [73], both strong and weak coupling features coexist, as studied recently theoretically. It indicates that the avoided crossing can be attributed to the Rabi doublet in the canonical strong coupling regime, with the unchanged CM energy near zero-detuning as a signature of the phonon-mediated collective states emission in the intermediate coupling regime [73, 74].

Specifically, in this coexisting strong and weak coupling regime, with increased phonon scattering as the bath temperature increases, each eigenstate derived by Jaynes–Cumming (JC) model experiences a different increase in the dephasing rate. The optical transition of lower and upper polaritons in the first rung of the JC ladder experiences less dephasing rate, which resembles the strong coupling feature and causes the observed avoided crossing of CM with X in our system. Simultaneously, the higher-order eigenstates experience larger dephasing and form a collective state [43, 44], located around the zero-detuning center, with the resultant unchanged CM energy around zero-detuning. Linewidth averaging is a canonical signature of the strong coupling regime, where the CM and X linewidths collapse to the averaged value due to their photon-matter polariton nature. As to the observed partially out-of-synchronization QD-CM linewidth averaging, it indicates the mixture of the collective state and fundamental Rabi doublet [73, 74], which perturbs the exciton-polariton linewidth averaging in the strong coupling regime.

From the point of view of the effective decay rate and cavity Q [75], the effective CM linewidth can be renormalized by an effective cavity pumping P_{CM} mainly resulting from phonon-mediated energy transfer from X to CM by $\Gamma_{\mathrm{CM}}^{\mathrm{eff}} = \gamma_{\mathrm{CM}} - P_{\mathrm{CM}}$. This resembles the CM linewidth narrowing when approaching the resonance. The reverse process applies to the effective linewidth broadening of X near the cavity resonance. We note here that our site-controlled single QD-cavity geometry safely excludes the spurious pumping terms from any parasitic QD and wetting layer in the P_{CM}, which commonly occurs in SK QDs. In addition, for the same cavity-QD with occasional CM energy shift as a result of the PhC cavity surface state changes, the avoided crossing can occur at lower temperatures such as 41 K. A slight blue shift of CM energy is observed as it crosses X when the temperature increases from 39.9 K to 41.6 K which suggests the repeatability of the collective states of the intermediate coupling regime in this QD-cavity device. This is detailed in supplementary section IV.

1.2. Span of degree-of-linear polarizations (DOLP) in the coexisting strong-weak intermediate coupling regime

To further investigate phonon-assisted coupling in the intermediate coupling regime, we performed the polarization-resolved detuning-dependent μPL on the same cavity-QD measured in figures 1 and 2 with controlled polarizers and bath temperature, as illustrated in figure 3(a). Here, the DOLP [36, 49], defined as $\mathrm{DOLP} = \frac{I_{\mathrm{V}} - I_{\mathrm{H}}}{I_{\mathrm{V}} + I_{\mathrm{H}}}$ where and I_{H} are the vertical- and horizontal-polarized μPL components align with TE and TM CMs respectively, is examined. The DOLP of different exciton species at various CM detuning serves as a probe to understand the pure dephasing mediated QD-CM coupling. Figure 3(b) summarizes the DOLP of X and excited LH at the detuning range covering the range in figure 2. It shows that the X and LH exciton species are co-polarized (positive DOLP) [49] with CM near resonance. It gradually loses the CM-like polarization (DOLP from +0.6 to 0) when detuned from resonance to $\approx \pm$ 1.2 meV detuning where the subsystem approaches the zero-DOLP (grey bar region).

Importantly, the detuning range for the pronounced co-polarization (DOLP > 0.5) corresponds to the detuning range (≈ -110 μeV to $+170$ μeV) where dramatic slope distortion appears in figure 2(b). At such detuning, the vertically polarized components of QD excitation can be transferred into the cavity decay channel as a result of the phonon-assisted coupling between the CM and QD [36, 38], leading to a relative depletion of the vertical-polarized QD μPL energies. Subsequently, such depletion enhances the vertical-polarized decay channel of QD itself by the Purcell-enhanced cavity photon channeling to the QD μPL energy, resulting in the significant co-polarized QD μPL of DOLP > 0.5 with the CM. Because the cavity loss rate is generally much larger than the QD radiative decay rate, we observe the overall co-polarization effect at detunings where QD and CM sufficiently interact. And the significant co-polarization is in roughly the same detuning range where the dramatic slope changes appear in figure 2(b), indicating the important contribution of the phonon-mediated Purcell enhancement in our observed coexisting strong-weak coupling regimes. The fact that the CM modifies the QD polarization only in a relatively small detuning range strongly suggests the absence of far-off-resonant coupling induced by wetting layers or background emissions. We further observed a negative DOLP at a much larger detuning range ($\approx$2 meV), which manifests an overall S-shape DOLP curve [48, 58], likely due to the intrinsic local density of states (LDOS) of the $L3$ cavity. The polarization-resolved measurements also enable the determination of the fine-structure splitting of X with orthogonal polarization, complying with the spin conservation selection rules. The inset of figure 3(b) shows this polarization dependence, with a resulting extracted X fine-structure splitting of $\approx$23 μeV.

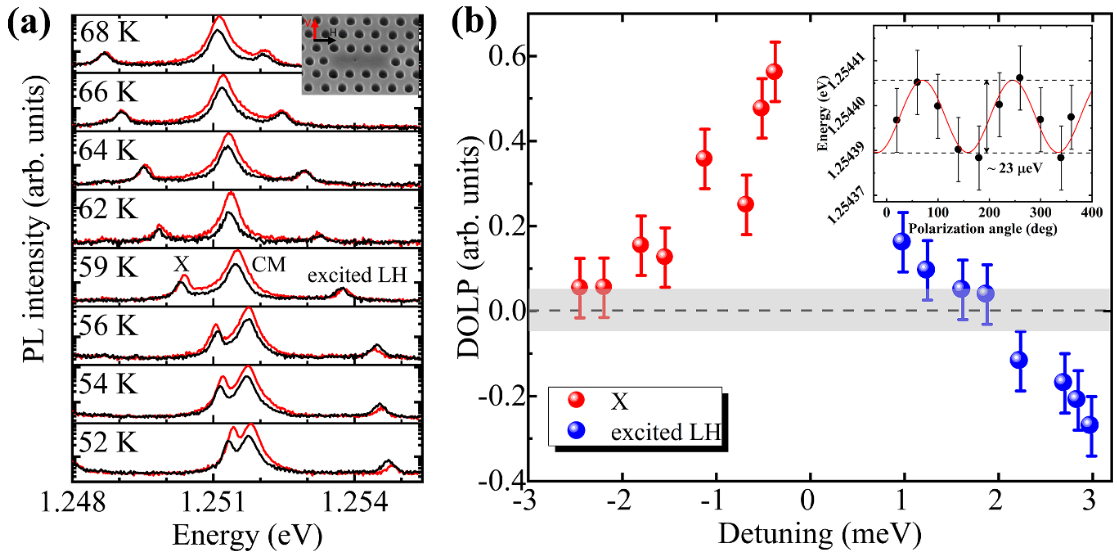

Figure 3. Phonon-assisted coupling examined by the degree of linear polarization (DOLP). (a) μPL spectrum resolved in H (black) and V (red) polarizations in the QD-CM detuning range from -3 meV to 3 meV. Inset: H and V polarization with respect to the cavity orientation. (b) DOLP of X and LH as a function of their detuning with respect to CM extracted from **a**. The black dash line marks the zero-DOLP line, and the grey bar region is the typical DOLP value for bare QDs without the presence of a cavity. Negative DOLP is observed over a much larger $\approx$2 meV detuning range, likely due to intrinsic LDOS of the *L*3 cavity. Detuning is defined as the energy difference with respect to CM. Measurements are with 532 nm CW excitation. Inset: X emission energy as a function of the half-wave plate fast-axis angle, indicative of the fine-structure splitting. The data deviates from a linear energy shift due to temperature drift during the measurement.

1.3. Anti-bunching and collective state photon statistics in the coexisting strong-weak intermediate coupling regimes

To study the radiative recombination dynamics of our coupled QD-cavity system, we measure the detuning-dependent decay time by TRPL on the X^- line as shown in figure 4(a). The X^- is chosen, instead of the X line, because it couples to the CM at relatively lower temperatures ($\approx$38 K) for which suppression of non-radiative recombination is more effective. When X^- is near resonance with the cavity under 160 μW excitation, Purcell enhancement results in a 1.2 ns decay time, extracted by the single-exponential decay convolved with an instrument response function of $\sim$500 ps. To examine the μPL decay of the X^- far-detuned from resonance ($\approx$6 K), the excitation power is doubled to obtain an adequate signal-to-noise ratio. The μPL rise time is clearly time-delayed [76], which arises from the finite *p*-state occupation under higher-power excitation. The extracted X^- off-resonance decay time increases up to 3.0 ns. We subsequently derive the Purcell factor [61] via: $\frac{\tau_0}{\tau_{X^-}(\delta)} = \frac{F_P\left(\kappa_{CM}+\gamma_{X^-}+\gamma_{leak}\right)^2}{4\delta^2+\left(\kappa_{CM}+\gamma_{X^-}+\gamma_{leak}\right)^2} f^2 + \frac{\tau_0}{\tau_{leak}}$, where $\tau_{X^-}(\delta) = 1.2$ ns is the X^- near-resonance lifetime, $\tau_{leak} = 3.0$ ns is the off-resonance X^- lifetime, $\tau_0 = 1$ ns is the typical bulk exciton lifetime, $\delta = 130$ μeV is the near-resonance detuning, $Q = 5500$ is the near-resonance Q factor, $\kappa_{CM} = 227$ μeV is the near-resonance cavity linewidth, and $\gamma_{X^-} = 311$ μeV is the X^- pure dephasing rate estimated from the FWHM of its off-resonance line. f is a dimensionless constant, which depends on the spatial alignment between the site-controlled QD and the cavity field maxima, and the orientation matching between the QD dipole and cavity field. The corresponding Purcell factor F_P for the case of ideal dipole alignment with respect to cavity field maximum is $\approx$2.46. The coupling strength can be estimated from $F_P = \frac{4|g|^2}{\left(\kappa_{CM}+\gamma_{X^-}+\gamma_{leak}\right)\gamma_0}$ [77] to be around 37 μeV.

To provide further insight into the coexisting strong-weak coupling regime, pump power-dependent photon statistics of the neutral exciton X coupled to the cavity are investigated by measuring the second-order correlation function $g^2(\tau)$ of the photon emission. As shown in figure 4(b), an anti-bunching feature ($g^2(0) < 1$) is presented as pump power varying from 300 to 800 nW, by subtracting the residual background photon detection. The raw histogram (in the unit of counts) is first normalized by the factor $\frac{T^2}{\Delta t(T-\tau)N^2}$, where T denotes the measurement time, Δt denotes the time bin, and N denotes the number of photon events [78]. Following [79]., to suppress the impact of detector dark counts and leaked photons from ambient and laser, the residual background photon is subtracted by considering the noise-influenced correlation function $g^2_{sub} = \left[g^2 - \left(1-\rho^2\right)\right]/\rho^2$, where ρ is the signal-to-background ratio. Eventually, we obtain $g^2(0) = 0.44$ at a lower pump power of 300 nW (onset of X saturation) and by simply considering a two-level system at low carrier injection. We fit the anti-bunching by a Gaussian convoluted expression

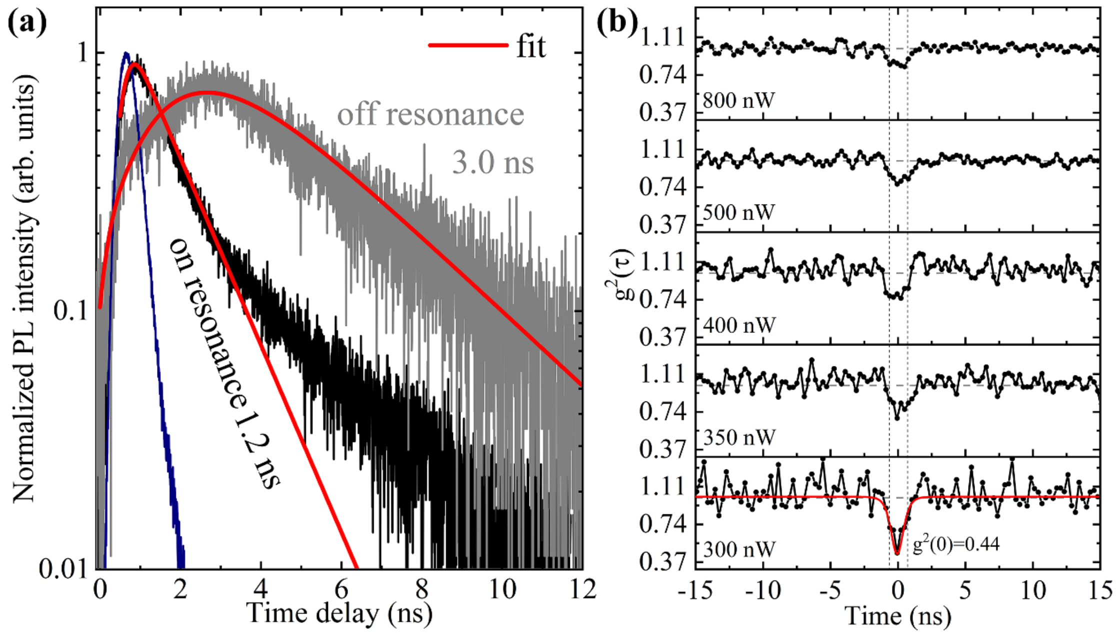

Figure 4. Exciton dynamics and photon statistics of the site-controlled QD-cavity subsystem in the coexisting strong-weak coupling regime. (a) Time-resolved μPL when X–is off- and on-resonance with the CM. The system instrument response is represented by the dark blue curve. The red curves are the single exponential fits. A 900 nm pulse laser is used for the excitation. (b) Second-order correlation function measured when X is in resonance with the CM under 532 nm excitation from 300 nW to 800 nW. The red curve is fit by a Gaussian convolved second-order autocorrelation function of a two-level system $g^2(\tau) = \int_{-\infty}^{\infty}\left(1-e^{-|t|/\tau_d}\right)\frac{e^{-\frac{(\tau-t)^2}{2\sigma^2}}}{\sigma\sqrt{2\pi}}\mathrm{d}t$where the FWHM of the Gaussian is equal to the timing jitter of the system 300 ps. The horizontal dash line indicates. The vertical dash lines indicate the region of the flattened antibunching bottom.

$g^2(\tau) = \int_{-\infty}^{\infty}\left(1-e^{-|t|/\tau_d}\right)\frac{e^{-\frac{(\tau-t)^2}{2\sigma^2}}}{\sigma\sqrt{2\pi}}\mathrm{d}t$ with the FWHM of the Gaussian equal to the timing jitter of the system 300 ps and τ_d is taken to be 400 ps. With such fitting parameters, the fit well reproduces the observed anti-bunching signature of the coupled X-CM emission at 300 nW. As the pump power increases up to 800 nW, we observe an increased $g^2(0)$ value up to 0.82. Note that the clean spectra of coupled X-CM after applying band pass filtering shown in figure S5 in supplementary section V indicates no emission from other excitonic species is involved in this measurement.

It is worth pointing out that the non-zero $g^2(0)$ at 300 nW even with the background subtraction can be due to limited phonon-assisted cavity feeding by X^- or LH-related transition, leading to an occasional uncorrelated photon. But this contribution is weak because the main emission feeding the cavity is X which is resonantly coupled to CM. Note that the *absence* of the wetting layer and parasite QDs in our single pyramidal QD rules out any cavity feeding from the excitonic continuum. On the other hand, the non-zero $g^2(0)$can be due to the short decay time (400 ps) which is comparable to the timing jitter of the HBT setup (300 ps). Further decreasing pump power can probably bring $g^2(0)$ closer to zero, which however is difficult to be measured due to low photon counts.

Moreover, with the increase of pump power, the antibunching dip gradually shows a plateau in contrast to the sharp dip at 300 nW. Note that we do not observe a bunching signature up to 800 nW at a larger time scale outside the antibunching notch which is reported by previous QD studies as a result of the detection of biexciton transition [80] or spectral diffusion [81]. It indicates that the cavity feeding by biexciton is limited in our measurement. Therefore, the increase of $g^2(0)$ by increased cavity feeding from biexciton can be ruled out. Instead, our tentative interpretation of the non-zero $g^2(0)$ and flattened antibunching bottom is that an increased pump power induces the elevated photon number accumulation in the cavity Fock states, and the resulting increased collective state [82] which can be ascribed to multiphoton emission dominates the photon statistics in the intermediate coupling regime and flatten the antibunching dip. The flattened antibunching bottom within a time window $\pm\tau$ suggests the probability of the resonantly coupled QD-cavity occupied with electron–hole pair is non-zero and remains unchanged up to a time delay τ after the first photon emission, which indicates the formation of collective states. The width of the antibunching notch, which indicates the population regeneration time of the collective states, not changing significantly with pump power suggests that the collective states and their population in higher rungs of the JC ladder are not saturated up to 800 nW. Our observed flattening of antibunched photon statistics is in line with the collective state resulting from phonon-mediated coupling in the intermediate coupling regime.

2. Conclusion

Precise positioning of single site-controlled inverted pyramidal InGaAs QDs at desired locations in PhC cavities provides great promise for functional monolithic quantum photonic circuits. However, the increased loss of PhC cavities based on (111)B-oriented GaAs membrane usually leads to the device operating at the weak coupling regime. In this study, we achieve the intermediate coupling regime of our single site-controlled inverted pyramidal InGaAs/GaAs QD—*L*3 PhC cavities, thanks to an increased cavity *Q*-factor compared to previous studies, by tailoring Indium content and pyramid size resulting in a red-shifted QD emission wavelength up to $\sim$1 μm. The detuning-dependent μPL spectrum reveals the trend of co-occurrence of QD-CM avoided crossing, which is a signature of Rabi doublet of the strongly coupled system, and the trend of keeping constant or slight blue shift of CM energy near zero-detuning due to the formation of collective states mediated by phonon-assisted coupling, and their partial out-of-synchronization linewidth-narrowing linked to their mixed behavior. Further polarization-resolved high-resolution μPL reveals the important contribution of phonon-mediated coupling in the coexisting strong-weak coupling regimes, in addition to the dynamical and anti-bunching photon statistical signatures. Overall, our work on achieving the intermediate coupling regime in site-controlled InGaAs QD-cavities suggests the feasibility of using such systems for quantum nodes in an integrated quantum photonic circuit for on-chip QIP and present a guideline for future improvement of the interaction strength and achieving the strong coupling regime for quantum states preparation, control, and nonlinear quantum optics.

Data availability statement

The data cannot be made publicly available upon publication because the cost of preparing, depositing and hosting the data would be prohibitive within the terms of this research project. The data that support the findings of this study are available upon reasonable request from the authors.

Acknowledgments

The authors thank helpful discussions with Abhinav Kumar Vinod, James F McMillan, Yujin Cho, Kai-Chi Chang, Jin Ho Kang, Justin Caram, and Baolai Liang from UCLA and technical help from Alexey Lyasota and Bruno Rigal from EPFL in the sample fabrication. J H, W L, and C W W acknowledge support from the National Science Foundation (1741707, 1936375, and 1919355). W L also acknowledges support from the Swiss National Science Foundation under Project 187963.

ORCID iDs

Jiahui Huang https://orcid.org/0000-0002-2249-6700
Wei Liu https://orcid.org/0000-0002-8637-4876
Murat Can Sarihan https://orcid.org/0000-0003-3800-7980
Chee Wei Wong https://orcid.org/0000-0001-7652-7720

References

[1] Ekert A K 1991 Quantum cryptography based on Bellâs Theorem *Phys. Rev. Lett.* **67** 661–3
[2] Dada A C, Leach J, Buller G S, Padgett M J and Andersson E 2011 Experimental high-dimensional two-photon entanglement and violations of generalized bell inequalities *Nat. Phys.* **7** 677–80
[3] Gao W B, Fallahi P, Togan E, Miguel-Sanchez J and Imamoglu A 2012 Observation of entanglement between a quantum dot spin and a single photon *Nature* **491** 426–30
[4] Weber J H, Kambs B, Kettler J, Kern S, Maisch J, Vural H, Jetter M, Portalupi S L, Becher C and Michler P 2019 Two-photon interference in the telecom c-band after frequency conversion of photons from Remote quantum emitters *Nat. Nanotechnol.* **14** 23–26
[5] Kim J-H, Aghaeimeibodi S, Carolan J, Englund D and Waks E 2020 Hybrid integration methods for on-chip quantum photonics *Optica* **7** 291
[6] Briegel H-J-J, Dür W, Cirac J I and Zoller P 1998 Quantum repeaters: the role of imperfect local operations in quantum communication *Phys. Rev. Lett.* **81** 5932–5
[7] Reinhard A, Volz T, Winger M, Badolato A, Hennessy K J, Hu E L and Imamoglu A 2011 Strongly correlated photons on a chip *Nat. Photon.* **6** 93–96
[8] Kim H, Bose R, Shen T C, Solomon G S and Waks E 2013 A quantum logic gate between a solid-state quantum bit and a photon *Nat. Photon.* **7** 373–7
[9] Sun S, Kim H, Luo Z, Solomon G S and Waks E 2018 A single-photon switch and transistor enabled by a solid-state quantum memory *Science* **361** 57–60
[10] He Y-M, He Y, Wei Y-J, Wu D, Atatüre M, Schneider C, Höfling S, Kamp M, Lu C-Y and Pan J-W 2013 On-demand semiconductor single-photon source with near-unity indistinguishability *Nat. Nanotechnol.* **8** 213–7

[11] Wang H *et al* 2019 Towards optimal single-photon sources from polarized microcavities *Nat. Photon.* **13** 770–5
[12] Nowak A K *et al* 2014 Deterministic and electrically tunable bright single-photon source *Nat. Commun.* **5** 3240
[13] Yoshle T, Scherer A, Hendrickson J, Khitrova G, Gibbs H M, Rupper G, Ell C, Shchekin O B and Deppe D G 2004 Vacuum rabi splitting with a single quantum dot in a photonic crystal nanocavity *Nature* **432** 200–3
[14] Hennessy K, Badolato A, Winger M, Gerace D, Atatüre M, Gulde S, Fält S, Hu E L and Imamoğlu A 2007 Quantum nature of a strongly coupled single quantum dot-cavity system *Nature* **445** 896–9
[15] Bose R, Cai T, Choudhury K R, Solomon G S and Waks E 2014 All-optical coherent control of vacuum rabi oscillations *Nat. Photon.* **8** 858–64
[16] Liu Y-C, Luan X, Li H-K, Gong Q, Wong C W and Xiao Y-F 2014 Coherent polariton dynamics in coupled highly dissipative cavities *Phys. Rev. Lett.* **112** 213602
[17] Gao J *et al* 2013 Strongly coupled slow-light polaritons in one-dimensional disordered localized States *Sci. Rep.* **3** 1–6
[18] Volz T, Reinhard A, Winger M, Badolato A, Hennessy K J, Hu E L and Imamoğlu A 2012 Ultrafast all-optical switching by single photons *Nat. Photon.* **6** 605–9
[19] Reithmaier J P, Sęk G, Löffler A, Hofmann C, Kuhn S, Reitzenstein S, Keldysh L V, Kulakovskii V D, Reinecke T L and Forchel A 2004 Strong coupling in a single quantum dot–semiconductor microcavity system *Nature* **432** 197–200
[20] Kasprzak J, Reitzenstein S, Muljarov E A, Kistner C, Schneider C, Strauss M, Höfling S, Forchel A and Langbein W 2010 Up on the Jaynes-Cummings ladder of a quantum-dot/microcavity system *Nat. Mater.* **9** 304–8
[21] Reithmaier J P 2008 Strong exciton–photon coupling in semiconductor quantum dot systems *Semicond. Sci. Technol.* **23** 123001
[22] Osada A, Ota Y, Katsumi R, Kakuda M, Iwamoto S and Arakawa Y 2018 Strongly coupled single quantum dot-cavity system integrated on a CMOS-processed silicon photonic chip *Phys. Rev. Appl.* **11** 024071
[23] Najer D *et al* 2019 A gated quantum dot strongly coupled to an optical microcavity *Nature* **575** 622–7
[24] Lodahl P, Mahmoodian S and Stobbe S 2013 Interfacing single photons and single quantum dots with photonic nanostructures *Rev. Mod. Phys.* **87** 347–400
[25] Englund D, Majumdar A, Faraon A, Toishi M, Stoltz N, Petroff P and Vučković J 2010 Resonant excitation of a quantum dot strongly coupled to a photonic crystal nanocavity *Phys. Rev. Lett.* **104** 073904
[26] Badolato A, Hennessy K, Atatüre M, Dreiser J, Hu E, Petroff P M and Imamoglu A 2005 Deterministic coupling of single quantum dots to single nanocavity modes *Science* **308** 1158–61
[27] Muller A, Fang W, Lawall J and Solomon G S 2009 Creating polarization-entangled photon pairs from a semiconductor quantum dot using the optical stark effect *Phys. Rev. Lett.* **103** 217402
[28] Xie Z *et al* 2015 Harnessing high-dimensional hyperentanglement through a biphoton frequency comb *Nat. Photon.* **9** 536–42
[29] Cheng X *et al* An efficient on-chip single-photon SWAP gate for entanglement manipulation *Conf. on Lasers and Electro-Optics FM2R.5 (OSA, 2020)* (https://doi.org/10.1364/CLEO_QELS.2020.FM2R.5)
[30] Liu J *et al* 2019 A solid-state source of strongly entangled photon pairs with high brightness and indistinguishability *Nat. Nanotechnol.* **14** 586–93
[31] Arsenault A C *et al* 2006 From colour fingerprinting to the control of photoluminescence in elastic photonic crystals *Nat. Mater.* **5** 179–84
[32] Sun S, Kim H, Solomon G S and Waks E 2016 A quantum phase switch between a single solid-state spin and a photon *Nat. Nanotechnol.* **11** 539–44
[33] Lindner N H and Rudolph T 2009 Proposal for pulsed on-demand sources of photonic cluster state strings *Phys. Rev. Lett.* **103** 113602
[34] Russo A, Barnes E and Economou S E 2018 Photonic graph state generation from quantum dots and color centers for quantum communications *Phys. Rev.* B **98** 085303
[35] Gimeno-Segovia M, Rudolph T and Economou S E 2019 Deterministic generation of large-scale entangled photonic cluster state from interacting solid state emitters *Phys. Rev. Lett.* **123** 070501
[36] Schwartz I, Schmidgall E R, Gantz L, Cogan D, Bordo E, Don Y, Zielinski M and Gershoni D 2015 Deterministic writing and control of the dark exciton spin using single short optical pulses *Phys. Rev.* X **5** 011009
[37] Schwartz I, Cogan D, Schmidgall E R, Don Y, Gantz L, Kenneth O, Lindner N H and Gershoni D 2016 Deterministic generation of a cluster state of entangled photons *Science* **354** 434–7
[38] Layden D, Chen M and Cappellaro P 2020 Efficient quantum error correction of dephasing induced by a common fluctuator *Phys. Rev. Lett.* **124** 020504
[39] Schöll E *et al* 2019 Resonance fluorescence of GaAs quantum dots with near-unity photon indistinguishability *Nano Lett.* **19** 2404–10
[40] Nawrath C, Olbrich F, Paul M, Portalupi S L, Jetter M and Michler P 2019 Coherence and indistinguishability of highly pure single photons from non-resonantly and resonantly excited telecom c-band quantum dots *Appl. Phys. Lett.* **115** 023103
[41] Auffèves A, Gerace D, Gérard J-M, Santos M F, Andreani L C and Poizat J-P 2010 Controlling the dynamics of a coupled atom-cavity system by pure dephasing *Phys. Rev.* B **81** 245419
[42] Bayer M and Forchel A 2002 Temperature dependence of the exciton homogeneous linewidth in (formula presented) self-assembled quantum dots *Phys. Rev.* B **65** 1–4
[43] Ates S, Ulrich S M, Ulhaq A, Reitzenstein S, Löffler A, Höfling S, Forchel A and Michler P 2009 Non-resonant dot–cavity coupling and its potential for resonant single-quantum-dot spectroscopy *Nat. Photon.* **3** 724–8
[44] Morreau A and Muljarov E A 2018 Phonon-induced dephasing in quantum dot-cavity QED *Phys. Rev.* B **100** 115309
[45] Roy C and Hughes S 2011 Influence of electron-acoustic phonon scattering on intensity power broadening in a coherently driven quantum-dot cavity system *Phys. Rev.* X **1** 1–19
[46] Roy C and Hughes S 2011 Phonon-dressed mollow triplet in the regime of cavity quantum electrodynamics: excitation-induced dephasing and nonperturbative cavity feeding effects *Phys. Rev. Lett.* **106** 247403
[47] Majumdar A, Kim E D, Gong Y, Bajcsy M and Vučković J 2011 Phonon mediated off-resonant quantum dot-cavity coupling under resonant excitation of the quantum dot *Phys. Rev.* B **84** 085309
[48] Jarlov C, Wodey E, Lyasota A, Calic M, Gallo P, Dwir B, Rudra A and Kapon E 2016 Effect of pure dephasing and phonon scattering on the coupling of semiconductor quantum dots to optical cavities *Phys. Rev. Lett.* **117** 076801
[49] Naesby A, Suhr T, Kristensen P T and Mørk J 2008 Influence of pure dephasing on emission spectra from single photon sources *Phys. Rev.* A **78** 045802
[50] Auffèves A, Gérard J M and Poizat J P 2009 Pure emitter dephasing: a resource for advanced solid-state single-photon sources *Phys. Rev.* A **79** 053838

[51] Cui G and Raymer M G 2006 Emission spectra and quantum efficiency of single-photon sources in the cavity-QED strong-coupling regime *Phys. Rev.* A **73** 053807
[52] Giesz V 2015 Cavity-enhanced photon-photon interactions with bright quantum dot sources *PhD thesis* Université Paris-Saclay
[53] Tawara T, Kamada H, Tanabe T, Sogawa T, Okamoto H, Yao P, Pathak P K and Hughes S 2010 Cavity-QED assisted attraction between a cavity mode and an exciton mode in a planar photonic-crystal cavity *Opt. Express* **18** 2719
[54] Winger M *et al* 2009 Explanation of photon correlations in the far-off-resonance optical emission from a quantum-dot-cavity system *Phys. Rev. Lett.* **103** 207403
[55] Toda Y, Moriwaki O, Nishioka M and Arakawa Y 1999 Efficient carrier relaxation mechanism in in GaAs/GaAs self-assembled quantum dots based on the existence of continuum States *Phys. Rev. Lett.* **82** 4114–7
[56] Vasanelli A, Ferreira R and Bastard G 2002 Continuous absorption background and decoherence in quantum dots *Phys. Rev. Lett.* **89** 216804
[57] Jarlov C Cavity quantum electrodynamics with systems of site-controlled quantum dots and photonic crystal cavities *PhD Thesis* École Polytechnique Fédérale de Lausanne (https://doi.org/10.5075/epfl-thesis-7039)
[58] Ćalić M 2013 Cavity quantum electrodynamics with site-controlled pyramidal quantum dots in photonic crystal cavities *PhD Thesis* École Polytechnique Fédérale de Lausanne (https://doi.org/10.5075/epfl-thesis-5957)
[59] Calic M *et al* 2011 Phonon-mediated coupling of InGaAs/GaAs quantum-dot excitons to photonic crystal cavities *Phys. Rev. Lett.* **106** 227402
[60] John S, Soukoulis C, Cohen M H and Economou E N 1986 Theory of electron band tails and the urbach optical-absorption edge *Phys. Rev. Lett.* **57** 1777–80
[61] Urbach F 1953 The long-wavelength edge of photographic sensitivity and of the electronic absorption of solids *Phys. Rev.* **92** 1324
[62] Delgoffe A M 2020 Functional elements for quantum-dot-based integrated quantum photonics *PhD thesis* École polytechnique fédérale de Lausanne (https://doi.org/10.5075/EPFL-THESIS-7533)
[63] Jarlov C, Gallo P, Calic M, Dwir B, Rudra A and Kapon E 2012 Bound and anti-bound biexciton in site-controlled pyramidal GaInAs/GaAs quantum dots *Appl. Phys. Lett.* **101** 191101
[64] Cade N I, Gotoh H, Kamada H, Nakano H and Okamoto H 2006 Fine structure and magneto-optics of exciton, trion, and charged biexciton states in single InAs quantum dots emitting at 1.3 μm *Phys. Rev.* B **73** 115322
[65] Muljarov E A and Zimmermann R 2004 Dephasing in quantum dots: quadratic coupling to acoustic phonons *Phys. Rev. Lett.* **93** 237401
[66] Ware M E, Stinaff E A, Gammon D, Doty M F, Bracker A S, Gershoni D, Korenev V L, Bădescu Ş C, Lyanda-Geller Y and Reinecke T L 2005 Polarized fine structure in the photoluminescence excitation spectrum of a negatively charged quantum dot *Phys. Rev. Lett.* **95** 177403
[67] Karlsson K F, Oberli D Y, Dupertuis M A, Troncale V, Byszewski M, Pelucchi E, Rudra A, Holtz P O and Kapon E 2015 Spectral signatures of high-symmetry quantum dots and effects of symmetry breaking *New J. Phys.* **17** 103017
[68] Johnsson M, Góngora D R, Martinez-Pastor J P, Volz T, Seravalli L, Trevisi G, Frigeri P and Muñoz-Matutano G 2019 Ultrafast carrier redistribution in single InAs quantum dots mediated by wetting-layer dynamics *Phys. Rev. Appl.* **11** 54043
[69] Baier M H, Malko A, Pelucchi E, Oberli D Y and Kapon E 2006 Quantum-dot exciton dynamics probed by photon-correlation spectroscopy *Phys. Rev.* B **73** 205321
[70] Dupertuis M A, Karlsson K F, Oberli D Y, Pelucchi E, Rudra A, Holtz P O and Kapon E 2011 Symmetries and the polarized optical spectra of exciton complexes in quantum dots *Phys. Rev. Lett.* **107** 127403
[71] Huber D, Lehner B U, Csontosová D, Reindl M, Schuler S, Covre Da Silva S F, Klenovský P and Rastelli A 2019 Single-particle-picture breakdown in laterally weakly confining GaAs quantum dots *Phys. Rev.* B **100** 235425
[72] Valente D, Suffczyński J, Jakubczyk T, Dousse A, Lemaître A, Sagnes I, Lanco L, Voisin P, Auffèves A and Senellart P 2014 Frequency cavity pulling induced by a single semiconductor quantum dot *Phys. Rev.* B **89** 041302
[73] Echeverri-Arteaga S, Vinck-Posada H and Gómez E A 2019 The strange attraction phenomenon in cQED: the intermediate quantum coupling regime *Optik* **183** 389–94
[74] Echeverri-Arteaga S, Vinck-Posada H and Gómez E A 2018 Explanation of the quantum phenomenon of off-resonant cavity-mode emission *Phys. Rev.* A **97** 043815
[75] Laussy F P, Del Valle E and Tejedor C 2009 Luminescence spectra of quantum dots in microcavities. I. bosons *Phys. Rev.* B **79** 235325
[76] Jarlov C, Lyasota A, Ferrier L, Gallo P, Dwir B, Rudra A and Kapon E 2015 Exciton dynamics in a site-controlled quantum dot coupled to a photonic crystal cavity *Appl. Phys. Lett.* **107** 191101
[77] Kim H, Sridharan D, Shen T C, Solomon G S and Waks E 2011 Strong coupling between two quantum dots and a photonic crystal cavity using magnetic field tuning *Opt. Express* **19** 2589
[78] PicoQuant GmbH QuCoa quantum correlation analysis software (available at: www.picoquant.com/products/category/software/qucoa-quantum-correlation-analysis-software)
[79] Brouri R, Beveratos A, Poizat J-P and Grangier P 2000 Photon antibunching in the fluorescence of individual color centers in diamond *Opt. Lett.* **25** 1294
[80] Kiraz A, Falth S, Becher C, Gayral B, Schoenfeld W V, Petroff P M, Zhang L, Hu E and Imamoglu A 2001 Photon correlation spectroscopy of a single quantum dot *Phys. Rev.* B **65** 161303
[81] Tamariz S, Callsen G, Stachurski J, Shojiki K, Butté R and Grandjean N 2020 Towards bright and pure single photon emitters at 300 k based on GaN quantum dots on silicon *ACS Photonics* **7** 1515–22
[82] Echeverri-Arteaga S, Vinck-Posada H, Villas-Bôas J M and Gómez E A 2020 Pure dephasing vs. phonon mediated off-resonant coupling in a quantum-dot-cavity system *Opt. Commun.* **460** 125115